Directing a Non-Heme Iron(III)-Hydroperoxide Species on a Trifurcated Reactivity Pathway

Wegeberg, Christina; Lauritsen, Frants R.; Frandsen, Cathrine; Mørup, Steen; Browne, Wesley R.; Mckenzie, Christine J.

Published in:
Chemistry - A European Journal

Link to article, DOI:
10.1002/chem.201704615

Publication date:
2018

Document Version
Publisher's PDF, also known as Version of record

Citation (APA):
Wegeberg, C., Lauritsen, F. R., Frandsen, C., Mørup, S., Browne, W. R., & Mckenzie, C. J. (2018). Directing a Non-Heme Iron(III)-Hydroperoxide Species on a Trifurcated Reactivity Pathway. *Chemistry - A European Journal*, *24*(20), 5134-5145. https://doi.org/10.1002/chem.201704615

ChemPubSoc Europe
DOI: 10.1002/chem.201704615
CHEMISTRY A European Journal
Full Paper

Coordination Chemistry |Hot Paper|

Directing a Non-Heme Iron(III)-Hydroperoxide Species on a Trifurcated Reactivity Pathway

Christina Wegeberg,[a] Frants R. Lauritsen,[a] Cathrine Frandsen,[b] Steen Mørup,[b] Wesley R. Browne,[c] and Christine J. McKenzie*[a]

In memory of Professor John J. McGarvey

Abstract: The reactivity of $[Fe^{III}(tpena)]^{2+}$ (tpena = *N,N,N′*-tris(2-pyridylmethyl)ethylenediamine-*N′*-acetate) as a catalyst for oxidation reactions depends on its ratio to the terminal oxidant H_2O_2 and presence or absence of sacrificial substrates. The outcome can be switched between: 1) catalysed H_2O_2 disproportionation, 2) selective catalytic oxidation of methanol or benzyl alcohol to the corresponding aldehyde, or 3) oxidative decomposition of the tpena ligand. A common mechanism is proposed involving homolytic O–O cleavage in the detected transient purple low-spin ($S = 1/2$) $[(tpenaH)Fe^{III}O–OH]^{2+}$. The resultant iron(IV) oxo and hydroxyl radical both participate in controllable hydrogen-atom transfer (HAT) reactions. Consistent with the presence of a weaker σ-donor carboxylate ligand, the most pronounced difference in the spectroscopic properties of $[Fe(OOH)(tpenaH)]^{2+}$ and its conjugate base, $[Fe(OO)(tpenaH)]^{+}$, compared to non-heme iron(III) peroxide analogues supported by neutral multidentate N-only ligands, are slightly blue-shifted maxima of the visible absorption band assigned to ligand-to-metal charge-transfer (LMCT) transitions and, corroborating this, lower Fe^{III}/Fe^{II} redox potentials for the pro-catalysts.

Introduction

Oxygen-coordinated iron complexes, such as iron(II)-O_2 (dioxygen), iron(III)-O_2 (superoxido and peroxido), iron(III)-OOH (hydroperoxido), and iron(III)-OOR (alkylperoxido), along with high-valent iron(IV) and iron(V) oxides formed upon homolytic or heterolytic cleavage of the O–O bond in these complexes, have been proposed as key catalytically competent intermediates in oxidations catalysed by heme[1,2] and non-heme[3,4] enzymes, as well as in synthetic model compounds.[3,5–8] To date, the field of non-heme peroxido compounds has been largely dominated by systems employing neutral aminopyridyl chelating ligands.[6,8] However, akin to the modulation of O_2 activation by heme enzymes mediated by a donor ligand *trans* to the oxygen binding site, we can reasonably expect that the introduction of anionic oxygen donors into the coordination sphere of an iron ion will stabilize higher oxidation states. Concomitantly, the O–O bond of peroxido ligands coordinated to the same iron centre will be weakened. This hypothesis is supported by the fact that many oxidation processes catalysed by non-heme iron O_2-activating enzymes, such as Rieske dioxygenases, tetrahydropterin-dependent hydroxylases, and 2-oxoglutarate-dependent dioxygenases and hydroxylases, possess an active site consisting of two histidine residues and one carboxylate group from Asp or Glu (Scheme 1). The reaction pathways followed by these enzymes proceed through cleavage of the O–O bond of peroxide/superoxide ligands derived from O_2 to form high-valent iron-oxido species, followed by direct oxidation of a substrate by the generated non-heme iron(IV).[4,9] Despite the biological precedence, the weakening of the O–O bond of an iron-coordinated peroxido ligand by the proximity of a carboxylato group has, to our knowledge, not yet been evaluated through systematic studies in model complexes.

Iron(III)-hydroperoxido and -peroxido complexes based on neutral pentadentate (N5) aminopolypyridyl ligands with an ethylenediamine backbone as the supporting scaffold, *N*-alkyl-*N,N′*-tris(2-pyridylmethyl)ethylenediamine (Rtpen; Scheme 2a) were the first systems for which peroxide derivatives were spectroscopically characterized, and these have been extensively studied.[10–18] Typically, these are generated by the reaction of air-stable iron(II) precursor complexes with H_2O_2, a prerequisite for which is oxidation of the iron centre from the Fe^{II} to the Fe^{III} oxidation state prior to formation of the Fe^{III}-OOH

[a] C. Wegeberg, Prof. F. R. Lauritsen, Prof. C. J. McKenzie
Department of Physics, Chemistry and Pharmacy
University of Southern Denmark, Campusvej 55
5230 Odense M (Denmark)
E-mail: mckenzie@sdu.dk

[b] Prof. C. Frandsen, Prof. S. Mørup
Department of Physics, Technical University of Denmark
2800 Kongens Lyngby (Denmark)

[c] Prof. W. R. Browne
Molecular Inorganic Chemistry, Stratingh Institute for Chemistry
University of Groningen, Nijenborgh 4
9747 AG, Groningen (The Netherlands)

Supporting information, including crystallographic tables as well as MIMS data and EPR and ^{1}H NMR spectroscopy data, and the ORCID numbers for the authors of this article can be found under https://doi.org/10.1002/chem.201704615.

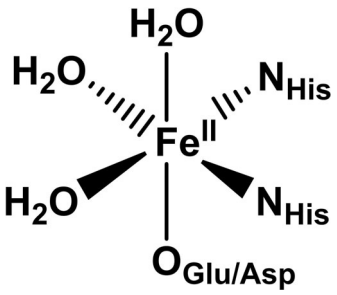

Scheme 1. Representation of the active site of O_2-activating non-heme iron enzymes. The water molecules are labile, allowing coordination of substrates (e.g., O_2, α-ketoglutarate, tetrahydropterin, isopenicillin N, taurine).

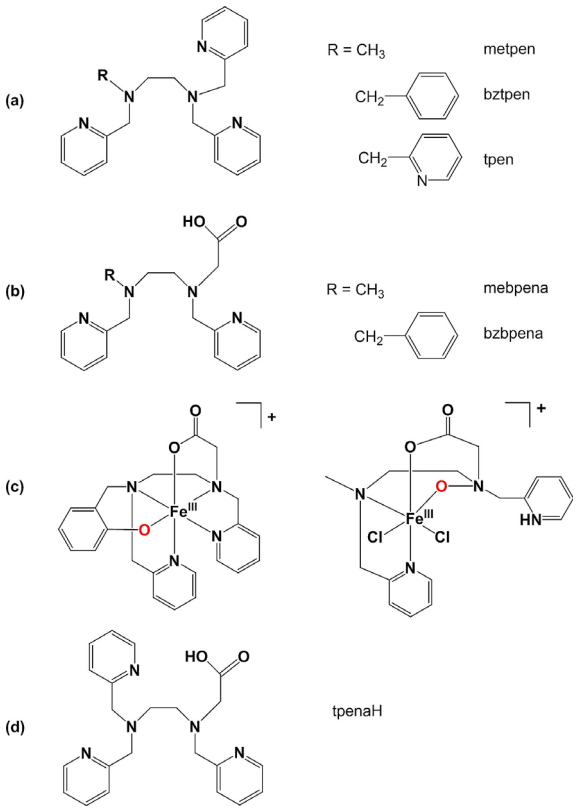

Scheme 2. Penta- and hexadentate ligands with ethylenediamine backbones for the preparation of iron(II/III/IV) peroxido and oxido complexes. a) Alkyl- and 2-methylpyridyl-containing N5 and N6 ligands, respectively. b) Alkyl and glycyl-containing N4O (Rbpena). c) The iron(III) complexes of the oxygenated ligands obtained from the reactions of the iron(III) complexes of bzbpena and mebpena with H_2O_2. d) Amino-pyridyl glycyl N5O ligand tpena/tpenaH used in this work.

species. Analogously to one of the functions of the protein in non-heme enzymes, the presence of more than four donors in these supporting ligands serves to inhibit hydrolytic polymerization reactions. This must be particularly important in the study of biologically relevant iron(III) chemistry in the presence of terminal oxidants such as peroxides. Purple transient Fe^{III} adducts, $[Fe^{III}(OOH)(Rtpen)]^{2+}$, have been observed at room temperature with half-lives of up to 2 h following their initial formation over several seconds (i.e., after the Fe^{II} to Fe^{III} oxidation step and coordination of a deprotonated H_2O_2 ligand). Kinetic studies with $[Fe^{III}(Rtpen)]^{2+}$ precursors have indicated that the reaction is essentially instantaneous when the metal pre-oxidation step is circumvented.[11] The Rtpen ligands also support iron(IV) oxo species. However, although their formation by homolytic cleavage of the O–O bond of peroxide precursors has been proposed, it is important to note that such species have not actually been prepared using H_2O_2 as the terminal oxidant, but instead by reaction of the Fe^{II} precursor with PhIO, *m*-CPBA, or ClO^-.[19]

Since monodentate carboxylate ligands are strong σ donors, we reasoned that iron(III) precursor compounds suitable for the rapid preparation of peroxido adducts would be accessed if one of the pyridyl arms were to be substituted by a biomimetic glycinate group. Our initial foray using this strategy produced the N4O ligands *N*-R-*N*,*N*′-bis(2-pyridylmethyl)ethylenediamine-*N*′-acetate (Rbpena), R = methyl, benzyl (Scheme 2 b), which indeed favoured the formation of iron(III) complexes.[18] Reactions of these iron(III) complexes with H_2O_2 (and alkyl peroxides or O_2 plus ascorbic acid) did not, however, produce detectable peroxide adducts, but instead oxygenation of the Rbpena ligands was observed. Aryl C–H oxidation of bzbpena gave the iron(III) complex, in which an O atom was installed in the ligand, *N*-(2-oxidobenzyl)-*N*,*N*′-bis(2-pyridylmethyl)ethylenediamine-*N*′-acetate, and O atom insertion into an Fe–N_{amine} bond provided an *N*-oxide ligand, 2-((2-(methyl(pyridin-2-ylmethyl)amino)ethyl)-oxido(pyridin-2-ylmethyl)azanyl)acetate (Scheme 2 c), for the iron(III) complex of the mepena ligand. These O atom C–H and Fe–N insertion reactions provide circumstantial evidence for the in situ formation of Fe^{III}-peroxide adducts and subsequent heterolytic Fe^{III}O–O(H) bond cleavage to give putative high-valent Fe^{V} oxo species capable of engaging in selective two-electron oxygen-atom transfer (OAT) reactions.

By adding a sixth heteroatom donor to replace the alkyl/aryl group in the N4O Rbpena ligand systems, namely a third pyridine group to give the N5O ligand *N*,*N*,*N*′-tris(2-pyridylmethyl)ethylenediamine-*N*′-acetate (tpena, Scheme 2 d), we demonstrate here that the ability to generate detectable transient iron(III)-peroxide adducts is reinstated. In other words, behaviour similar to that observed for the iron(III) complexes of N5 Rtpen can be observed, and this contrasts with that for the iron(III) complexes of N4O Rbpena. However, the Fe^{III}-OOH species formed from the tpena-iron complex has a significantly shorter lifetime than those derived from the corresponding Rtpen-based systems. At first sight, it might seem surprising that the ostensibly coordinatively saturated iron(III) precursor $[Fe(tpena)]^{2+}$ can form heteroleptic complexes with co-ligand peroxide donors. However, we have previously demonstrated that external substrates can be selectively oxidized using the terminal oxygen-atom-transfer reagents iodosylbenzene and *N*-morpholine-*N*-oxide catalysed by $[Fe(tpena)]^{2+}$, and a seven-coordinated intermediate heteroleptic Fe^{III}-oxidant adduct was isolated.[20,21]

Herein, we demonstrate the formation and characterization of the species $[(tpenaH)Fe^{III}\text{-}OOH]^{2+}$ and $[(tpenaH)Fe^{III}\text{-}OO]^{+}$ and show that the reactivity of these complexes is highly de-

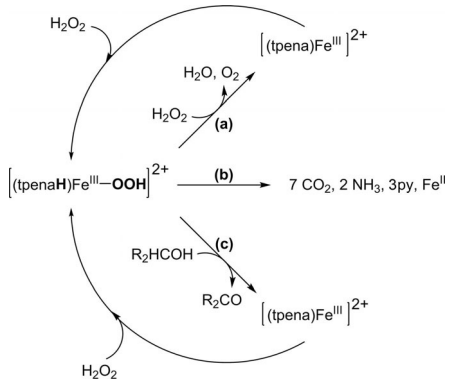

Scheme 3. Trifurcation of reactivity for the dihydrogen peroxide adduct of the iron(III) complex of tpena: a) catalytic H_2O_2 disproportionation, b) tpena degradation, c) catalytic alcohol oxidation to aldehydes.

pendent on opportunity (Scheme 3); specifically, we show that the complex elicits efficient disproportionation of H_2O_2, but crucially, the turnover catalytic conversion of H_2O_2 can be bifurcated[22] and in the presence of oxidizable substrates such as methanol or benzyl alcohol the oxidizing power is highly efficiently directed towards these substrates. A third path of oxidative chemistry has also been observed, namely destructive oxidation of the tpena ligand when the ratio of H_2O_2 to $[Fe(tpena)]^{2+}$ is low, for example, in the final stages of H_2O_2 disproportionation or if the concentration of substrate alcohol is lower than that of H_2O_2. The present study highlights the potential of the tpena ligand system in supporting various metal(III) coordination numbers (6 and 7), geometries, and spin states, as well as flexible stereochemistry in terms of the number of donor atoms furnished by tpenaH/tpena (5 or 6). The results emphasize the potential role played by a single biomimetic carboxylate donor moiety along with a second pendant pyridine base in the coordination sphere.

Results and Discussion

Fe^{III}/Fe^{II} redox potentials for analogous iron complexes of N5O and N6 ligands

Solutions of $[Fe^{III}(tpena)]^{2+}$ in acetonitrile are obtained by the dehydration of $[(tpenaH)Fe(\mu\text{-}O)Fe(tpenaH)]^{4+}$ upon dissolution:[21] $[(tpenaH)Fe(\mu\text{-}O)Fe(tpenaH)]^{4+} \rightarrow 2\ [Fe(tpena)]^{2+} + H_2O$.

The cyclic voltammogram of $[Fe^{III}(tpena)]^{2+}$ in acetonitrile shows a broad wave due to overlapping reversible Fe^{III}/Fe^{II} redox couples at 0.02 V and 0.06 V vs Fc/Fc^+ (Figure 1 a). The redox waves are associated with the high-spin ($S = {}^5/_2$) *mer*-py_3-$[Fe(tpena)]^{2+/+}$ and low-spin ($S = {}^1/_2$) *fac*-py_3-$[Fe(tpena)]^{2+/+}$ diastereoisomers (Figure 1 b). Both the *mer*-py_3 and *fac*-py_3 isomers have been previously identified in both the solid and solution states by Mössbauer spectroscopy and in the frozen-solution state by EPR spectroscopy.[21] The potentials are 0.38 and 0.34 V lower compared to that for the Fe^{III}/Fe^{II} couple of $[Fe(tpen)]^{3+/2+}$ (0.40 V vs. Fc/Fc^+, tpen = *N,N,N′,N′*-tetrakis(2-pyridylmethyl)ethylenediamine; Figure 1 b). This result is consistent with our expectation that the binding of a negatively charged carboxylate group in place of a pyridyl moiety will stabilize higher iron oxidation states. It is also consistent with the tendency, in the presence of air, for the tpen and neutral N5 Rtpen ligands to form iron(II) complexes, whereas iron(III) complexes are formed with tpena, irrespective of the oxidation state of the precursor iron starting salt (+2 or +3). The minor redox wave at 0.46 V is due to the oxo-bridged precursor, $[(tpenaH)Fe(\mu\text{-}O)Fe(tpenaH)](ClO_4)_4$.[23]

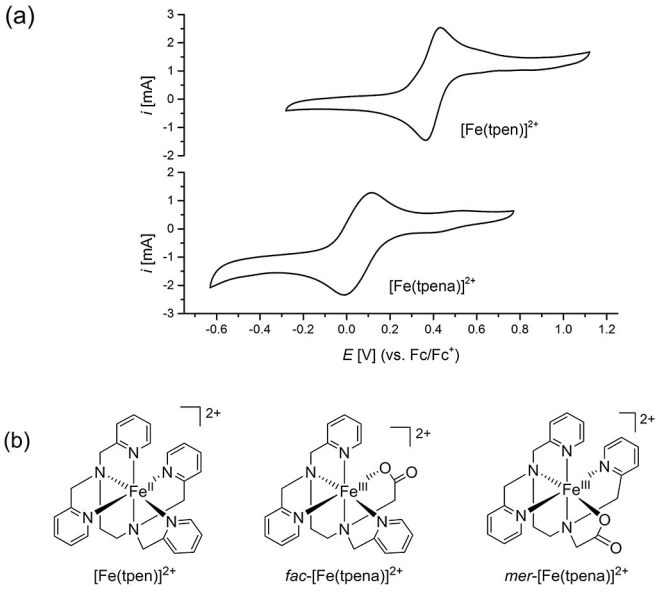

Figure 1. a) Cyclic voltammetry of $[Fe^{II}(tpen)]^{2+}$ (N_6 ligand) and $[Fe^{III}(tpena)]^{2+}$ (N_5O ligand) formed in situ from $[Fe^{II}(tpen)](ClO_4)_2$ and $[(tpenaH)Fe^{III}(\mu\text{-}O)Fe^{III}(tpenaH)](ClO_4)_4$, respectively. [Fe] = 0.5 mM. Scan rate 0.1 V s^{-1} in CH_3CN (0.1 M $TBAClO_4$). b) Structures of $[Fe(tpen)]^{2+}$, *fac*-$[Fe(tpena)]^{2+}$, and *mer*-$[Fe(tpena)]^{2+}$.

Reaction of HCl and H_2O_2 with $[Fe(tpena)]^{2+}$ to form $[FeX(tpenaH)]^{2+}$ ($X = Cl^-$, OOH^-)

Addition of concentrated HCl to solutions of either the brown complex $[(tpenaH)Fe(\mu\text{-}O)Fe(tpenaH)]^{4+}$ (in water/EtOH) or of the red-orange complex $[Fe(tpena)]^{2+}$ (in acetonitrile) resulted in immediate formation of $[Fe(Cl)(tpenaH)]^{2+}$, as manifested by a colour change to yellow, $\lambda_{max} = 312$ and 361 nm [Eqs. (1 a) and (1 b), respectively].

$$[(tpenaH)Fe(\mu\text{-}O)Fe(tpenaH)]^{4+} + 2\,HCl \rightarrow 2\,[Fe(Cl)(tpenaH)]^{2+} + H_2O \quad (1a)$$

$$fac/mer\text{-}[Fe(tpena)]^{2+} + HX \rightarrow FeX(tpenaH)]^{2+} \qquad X = Cl^-,\ OOH^- \quad (1b)$$

The single-crystal X-ray structure of $[Fe(Cl)(tpenaH)](ClO_4)_2 \cdot EtOH \cdot 2\,H_2O$ (Figure 2 a) shows that the iron(III) ion is pentacoordinated by tpenaH, with a chlorido ligand occupying the sixth site. The pyridine arm attached to the same amine group, as the glycyl arm does not coordinate to the iron(III)

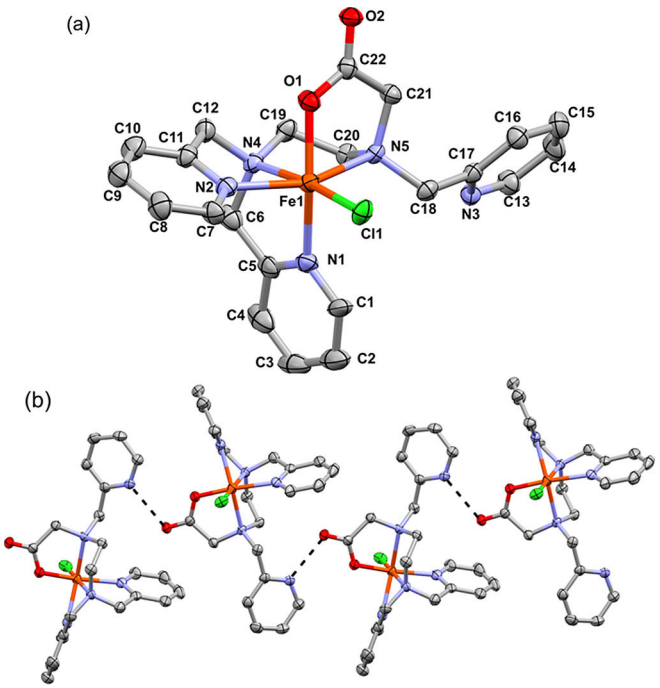

Figure 2. a) Crystal structure of $[Fe(Cl)(tpenaH)]^{2+}$. b) The hydrogen-bonded 1D helical chain of cations parallel to the *b*-axis. Thermal ellipsoids are drawn at 50% probability and the protons are omitted for clarity. The intermolecular hydrogen bond is shown with dashed lines (C=O···H–N_{py} 1.845 Å).

centre and is protonated. The structure is consistent with the chlorido ligand taking the position that the dangling pyridine had occupied in *fac*-$[Fe(tpena)]^{2+}$. The chlorido ligand is *trans* to the tertiary amine bearing the two methylpyridyl groups and *cis* to the carboxylato moiety. This structure is one (A) of the six possible diastereoisomers depicted in Scheme 4. Intermolecular hydrogen bonding (Figure 2b) between the non-coordinated carboxylato oxygen and the protonated pyridine results in 1D homochiral chains of the cations parallel to the *b*-axis. These chains are separated by stacks of ClO_4^- anions, and water and ethanol molecules occupy pockets between the cationic chains. The solid-state Mössbauer spectrum of $[Fe(Cl)(tpenaH)](ClO_4)_2$·EtOH·2$H_2O$ shows a broad singlet at $\delta = 0.46\ mm\,s^{-1}$, consistent with a high-spin ($S = 5/2$) iron(III) complex. $[Fe(Cl)(tpenaH)](ClO_4)_2$·EtOH·2$H_2O$ is hygroscopic, and we have speculated that this could be associated with hydrolysis and loss of HCl to form the pseudo aquo complex $[Fe(OH)(tpenaH)]^{2+}$, which has been identified in aqueous solutions at low pH.[23,24]

Addition of H_2O_2 to $[Fe(tpena)]^{2+}$ in acetonitrile resulted in an immediate colour change from red to purple, indicative of the formation of an Fe^{III}-hydroperoxido adduct structurally analogous to the HCl adduct, namely $[Fe^{III}(OOH)(tpenaH)]^{2+}$ [Eq. (1b)]. The concentration of the transient peroxido complex in acetonitrile is maximized under conditions that minimize the concentration of the hemihydrate, $[(tpenaH)Fe(\mu\text{-}O)Fe(tpenaH)]^{4+}$, supporting the view that the anhydrate $[Fe(tpena)]^{2+}$ is the immediate precursor for reaction with H_2O_2. Purple solutions of $[Fe^{III}(OOH)(tpenaH)]^{2+}$ in acetonitrile, decay over 30 s at room temperature and over several hours at −40 °C. The rate of decay for $[Fe^{III}(OOH)(tpenaH)]^{2+}$ is significantly faster than that for $[Fe^{III}(OOH)(metpen)]^{2+}$ generated in methanol from $[Fe(metpen)Cl](PF_6)$ with 50 equiv of H_2O_2 at room temperature. Of relevance to the oxidizing ability of $[Fe^{III}(OOH)(tpenaH)]^{2+}$ (see below) is that it cannot be observed in methanol; this is in stark contrast to the $[Fe^{III}(OOH)(Rtpen)]^{2+}$ complexes, for which methanol is the favoured solvent for generation.

Spectroscopic properties of $[Fe(OOH)(tpenaH)]^{2+}$

The transient purple species, assigned as $[Fe^{III}(OOH)(tpenaH)]^{2+}$ shows an absorption band at 520 nm ($\varepsilon = 465\ M^{-1}\,cm^{-1}$), consistent with an $Fe^{3+} \leftarrow ROO^-$ charge-transfer transition (Figure 3a, red curve). The Raman spectrum elicited at $\lambda_{exc} = 532$ nm shows resonantly enhanced bands at 613 and 788 cm^{-1} (Figure 3b), which can be assigned to Fe–O and O–O stretching modes, respectively, by comparison with previous literature; see Table 1. The EPR spectrum of a frozen solution shows a rhombic signal ($g = 2.21$, 2.15, 1.96; Figure 3c). The frozen-solution-state Mössbauer spectrum displays a doublet with $\delta = 0.21\ mm\,s^{-1}$ and $\Delta E_Q = 2.08\ mm\,s^{-1}$ (14%, Figure 3d), which is consistent with a low-spin Fe^{III} species. The spectrum also shows the presence of the EPR-silent starting complex $[(tpenaH)Fe\text{-}O\text{-}Fe(tpenaH)]^{4+}$ ($\delta = 0.43\ mm\,s^{-1}$, $\Delta E_Q = 1.63\ mm\,s^{-1}$, 14%).[21] The structure of $[Fe^{III}(OOH)(tpenaH)]^{2+}$ can be any of six diastereoisomers (Scheme 4). However, the simplicity of the Raman, Mössbauer, and EPR spectra implies that one of these isomers dominates, notwithstanding the possibility that the differences between the stereoisomers are insufficient to cause significant changes in the vibrational, nuclear, and spin characteristics. In the present study, the precise stereochemistry of the intermediate is not of specific concern and for simplicity of the data analyses, it is assumed that a single diastereoisomer of $[Fe^{III}(OOH)(tpenaH)]^{2+}$ is formed, cor-

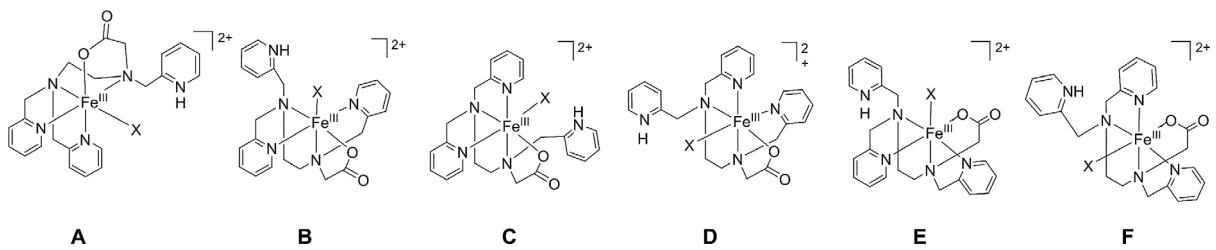

Scheme 4. Possible diastereoisomers of $[Fe(X)(tpenaH)]^{2+}$; X = Cl^-, OH^-, OOH^-.

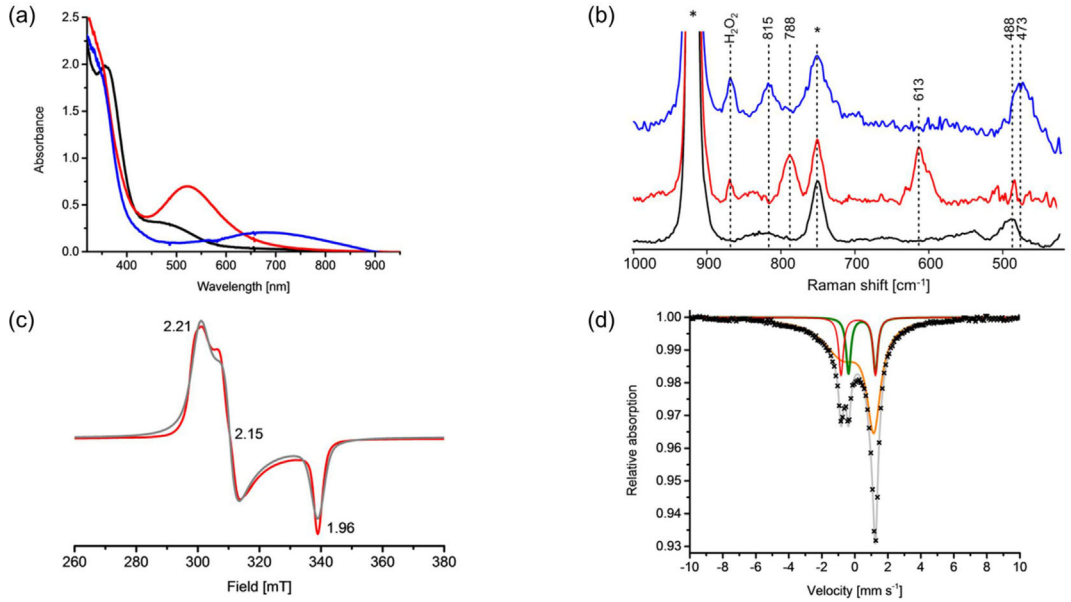

Figure 3. Solution-state spectroscopic characterization of $[Fe(OOH)(tpenaH)]^{2+}$ and $[Fe(OO)(tpenaH)]^{+}$. Colour coding: $[Fe(tpena)]^{2+}$ in black, $[Fe(OOH)(tpenaH)]^{2+}$ in red, $[Fe(OO)(tpenaH)]^{+}$ in blue, $[Fe_2O(tpenaH)_2]^{4+}$ in green. Unidentified species depicted in orange (see text). The sum of the fitted data is coloured in grey. $[Fe(OOH)(tpenaH)]^{2+}$ was generated by addition of 50 equiv of H_2O_2 to $[Fe(tpena)]^{2+}$ in MeCN, and subsequent addition of 30 equiv of Et_3N gave $[Fe(OO)(tpenaH)]^{+}$. a) UV/Vis absorption spectra (RT, [Fe] = 1.5 mM). b) Resonance Raman spectra (−30 °C, [Fe] = 3 mM, λ_{exc} = 532 nm for $[Fe(OOH)(tpenaH)]^{2+}$ and λ_{exc} = 691 nm for $[Fe(OO)(tpenaH)]^{+}$). All spectra were normalized to the solvent band at 750 cm^{-1}. * = solvent bands. c) X-band EPR spectrum of $[Fe(OOH)(tpenaH)]^{2+}$ (microwave frequency 9.314542 GHz, 110 K, [Fe] = 2 mM, fit in grey). d) Mössbauer spectrum of a mixture containing $[Fe(OOH)(tpenaH)]^{2+}$ (14%), $[Fe_2O(tpenaH)_2]^{4+}$ (14%), and unidentified species (72%) ([Fe] = 2 mM).

responding to that observed in the crystal structure of the HCl adduct, Figure 2 (i.e., A in Scheme 4).

Deprotonation of $[Fe(OOH)(tpenaH)]^{2+}$

The addition of NEt_3 (30 equiv) to solutions of $[Fe^{III}(OOH)(tpenaH)]^{2+}$ and excess H_2O_2 in acetonitrile results in an instant colour change from purple to blue and the appearance of a new absorption band at 675 nm (Figure 3 a, blue line). The lifetime of the new species is about 10 min at 0 °C when generated from 50 equiv of H_2O_2 and 30 equiv of Et_3N. Immediate loss of the Fe–O and O–O bands of the end-on Fe^{III}-OOH in the Raman spectrum is accompanied by the appearance of the corresponding bands of a side-on peroxido complex at 473 and 815 cm^{-1} (Figure 3 b), consistent with assignment of the species as $[Fe^{III}(OO)(tpenaH)]^{+}$. The band positions are close to those reported for $[Fe^{III}(OO)(tpen)]^{+}$ and $[Fe^{III}(OO)(metpen)]^{+}$ (Table 1). A high-spin signal (g^{eff} = 8.8, 5.0, 4.3, 4.2, 3.5) appears in the EPR spectrum (Figure 4 a). The Mössbauer spectrum (Figure 4 b) of a sample composed of ^{57}Fe-labelled $[Fe^{III}(tpena)]^{2+}$ shows a doublet with δ = 0.48 mm s^{-1} and ΔE_Q = 1.21 mm s^{-1} (47%), which is consistent with a high-spin Fe^{III} species. The doublet due to $[Fe(OOH)(tpenaH)]^{2+}$ is not observed, and the spectrum also shows the presence of a significant amount of the EPR-silent starting material $[(tpenaH)Fe\text{-}O\text{-}Fe(tpenaH)]^{4+}$ (δ = 0.46 mm s^{-1}, ΔE_Q = 1.68 mm s^{-1}, 53%).[21] It is interesting to note that this spectrum does not show the presence of unidentified iron complexes derived from the decomposition of tpena (see below) in contrast to the spectrum for $[Fe(OOH)(tpenaH)]^{2+}$ (Figure 3 d). This lack of decomposition might suggest that the peroxide species is less reactive than the hydroperoxide species. This idea is supported by the fact that in order to acquire this clean spectrum it was necessary to add the base before the H_2O_2,

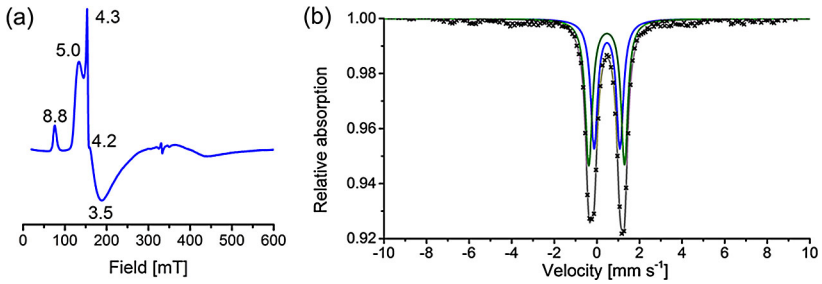

Figure 4. Frozen-solution-state spectroscopic characterization of $[Fe(OO)(tpenaH)]^{+}$ (blue). a) EPR spectrum (microwave frequency 9.315392 GHz, 110 K, 2 mM $[Fe(tpena)]^{2+}$ and 50 equiv of H_2O_2 followed by 30 equiv of Et_3N). b) Mössbauer spectrum of a solution containing $[Fe(OO)(tpenaH)]^{+}$ (blue, 47%) and $[Fe_2O(tpenaH)_2]^{4+}$ (green, 53%). Fitting in grey ($[^{57}Fe]$ 2 mM, 30 equiv of Et_3N followed by 50 equiv of H_2O_2).

Table 1. Spectroscopic properties of $[(tpenaH)Fe\text{-}O\text{-}Fe(tpenaH)]^{4+}$, *fac*-$[Fe(tpena)]^{2+}$, *mer*-$[Fe(tpena)]^{2+}$, $[Fe(OOH)(tpenaH)]^{2+}$, $[Fe(OO)(tpenaH)]^{+}$, and related Fe^{III}-hydroperoxo and peroxo complexes of neutral N5 and N6 donor ligands.

	UV/Vis[a]		rRaman[a]			Mössbauer[a]		EPR[a,b]		
	λ_{max} [nm]	ε [M^{-1} cm^{-1}]	$\nu_{Fe\text{-}O}$ [cm^{-1}]	$\nu_{O\text{-}O}$ [cm^{-1}]	Exp. conditions	δ [$mm\,s^{-1}$]	ΔE_Q [$mm\,s^{-1}$]	*g*-values	*S*	Ref.
$[Fe^{III}{}_2O(tpenaH)_2)]^{4+}$	258		830	n/a	solid state	0.43	1.63	silent	$^5/_2$	[24], this work
fac-$[Fe^{III}(tpena)]^{2+}$	360[c]	1330[c]				0.18	2.26	2.74, 2.29, 1.68	$^1/_2$	[21]
mer-$[Fe^{III}(tpena)]^{2+}$	[c]	[c]				0.25		4.20	$^5/_2$	[21]
$[Fe^{III}Cl(tpenaH)]^{2+}$	361, 312	4150, 3940			solid state	0.46			$^5/_2$	this work
$[Fe^{III}(OOH)(tpenaH)]^{2+}$	520	465[d,f]	613	788	MeCN, −30 °C, λ_{exc} 532 nm	0.21	2.08[e]	2.21, 2.15, 1.96	$^1/_2$	this work
$[Fe^{III}(OOH)(tpen)]^{2+}$	541	900,[f] 200[g]	617	796	MeOH, RT, λ_{exc} 568 nm			2.22, 2.15, 1.97	$^1/_2$	[14], this work
$[Fe^{III}(OOH)(metpen)]^{2+}$	537	1000,[f] 260[g]	617	796	MeOH, RT, λ_{exc} 568 nm	0.19	−2.01[e]	2.19, 2.12, 1.95	$^1/_2$	[10, 14, 15], this work
$[Fe^{III}(OOH)(bztpen)]^{2+}$	542					0.17	−2.07[e]	2.20, 2.16, 1.96	$^1/_2$	[11, 16]
$[Fe^{III}(OO)(tpenaH)]^{+}$	675	140[d]	473	815	MeCN, −30 °C, λ_{exc} 691 nm	0.48	1.21	8.8, 5.0, 4.3, 4.2, 3.5	$^5/_2$	this work
$[Fe^{III}(OO)(tpen)]^{+}$	755	450	470	817	MeOH, RT, λ_{exc} 647 nm			7.5, 5.9	$^5/_2$	[14]
$[Fe^{III}(OO)(metpen)]^{+}$	740	500	470	819	MeOH, RT, λ_{exc} 647 nm	0.64	1.37	7.5, 5.9, 4.4	$^5/_2$	[12, 14, 15]
$[Fe^{III}(OO)(bztpen)]^{+}$	770					0.63	1.12	7.60, 5.74	$^5/_2$	[11, 16]

[a] Data on tpena-based complexes were recorded in MeCN; all other complexes were examined in MeOH. In the case of UV/Vis absorption data, caution should be exercised in direct comparison of the molar absorptivities of Fe^{III} peroxide complexes with those in the literature due to their reactivity under the experimental conditions (temperature, water concentration, purity, etc.), which will affect lifetimes. [b] g^{eff} are denoted for $S = {}^5/_2$. All *g* values were determined with X-band frequencies. [c] The UV/Vis absorption spectra of the two diastereoisomers *fac*-$[Fe(tpena)]^{2+}$ and *mer*-$[Fe(tpena)]^{2+}$ are dominated by the former, based on analysis of Mössbauer spectroscopic data.[21] [d] Molar absorptivities were calculated using solutions showing the maximum chromophore absorbance achieved with 50 equiv of H_2O_2 at RT in MeCN. [e] The signs of the quadrupole splittings for $[Fe(OOH)(metpen)]^{2+}$ and $[Fe(OOH)(bztpen)]^{2+}$ were determined by applied parallel field Mössbauer spectroscopy; similar data for $[Fe(OOH)(tpena)]^{2+}$ are not available. [f] Reported molar absorptivities determined from spectra of the $Fe^{III}OOH$ and $Fe^{III}OO$ (peroxido) species prepared by reaction of the relevant 1 mM Fe^{II} precursor with 100 equiv of H_2O_2 (and an additional three equiv. of Et_3N for $Fe^{III}OO$), according to the references cited. [g] Measured under the same conditions as those applied to observe $[Fe^{III}(OOH)(tpena)]^{2+}$ and $[Fe^{III}(OO)(tpenaH)]^{+}$ in this work ($[Fe^{III}(tpena)]^{2+}$ with 50 equiv of H_2O_2 or 50 equiv of H_2O_2 plus 30 equiv of Et_3N, respectively). Calculated extinction coefficients for labile species should always be taken with caution, and it should be noted that we have observed that decay rates, and hence visible-light absorption, depend on concentration. This (and differences in handling) explain the difference between the molar absorptivities calculated from our measurements and those in the literature, which are otherwise internally consistent.

followed by rapid freezing in liquid N_2. This protocol meant that the presumably more labile $[Fe(OOH)(tpenaH)]^{2+}$ did not get the chance to form in any significant concentration.

Spectroscopic data for $[Fe(tpena)]^{2+}$ peroxide adducts are consistent with a side-on bound peroxide Fe^{III} complex in $[Fe^{III}(OO)(tpenaH)]^{+}$ by comparison with iron complexes of Rtpen (Table 1, R = Me, $BzCH_2$, $PyCH_2$). This species is potentially intramolecularly (Scheme 5) or intermolecularly H-bonded, with the solid-state structure of $[Cr(\eta^2\text{-}OO)(tpenaH)]^{+}$ furnishing a structural analogue for the latter.[25] The pendant pyridinium moiety of the tpenaH ligand is a second site available for deprotonation by a base, and $[Fe^{III}(OO)(tpena)]$ is a plausible product from the reaction of $[Fe^{III}(OOH)(tpenaH)]^{2+}$ with two equivalents of base (Scheme 5). However, in this situation, the pyridine is expected to re-coordinate to the iron atom to form a seven-/eight-coordinated product for η^1- and $\eta^2\text{-}OO^{2-}$, respectively. This is not expected to be sterically too demanding, because the N-Fe-N angles for multidentate ligands with ethylenediamine backbones are generally less than 90°, thereby providing a relatively open face on the opposite side of the metal ion. Indeed, heptacoordination has been structurally characterized in the high-spin d^5 metal ion complexes $[Fe(OIPh)(tpena)](ClO_4)_2$[20] and $[Mn(OH_2)(tpena)](ClO_4)_2$.[26] The relatively open face presented by tpena in these structures suggests that formation of a heteroleptic complex with an η^2-diatomic ligand is also a reasonable structure for the peroxido complex, especially since $\eta^2\text{-}OO^{2-}$ ligands are no more sterically demanding than monodentate oxide (O^{2-}) ligands.[27] Addition of further base leads to the formation of yellow solutions, with vigorous decomposition of H_2O_2 and ultimately decomposition of the complex (see below), such that the precise details of the protonation state cannot be readily determined experimentally.

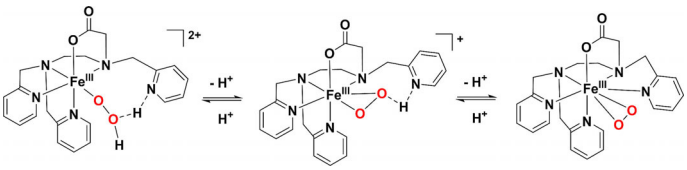

Scheme 5. Single- and double-deprotonation of $[Fe(OOH)(tpenaH)]^{2+}$, leading to side-on peroxide coordination with speculative intramolecular hydrogen bonding.

Consideration of Table 1 shows that the most significant spectroscopic difference is that the $Fe^{3+} \leftarrow OOH^{-}$ and $Fe^{3+} \leftarrow OO^{2-}$ LMCT bands for the end-on hydroperoxido and side-on peroxido Fe^{III}-tpena complexes are at shorter wavelengths than those for the analogous Rtpen-based complexes. The

λ_{max} for $[Fe(OOH)(tpenaH)]^{2+}$ is hypsochromically shifted by about 20 nm, and the λ_{max} for $[Fe^{III}(OO)(tpenaH)]^{+}$ is shifted by 60, 75, and 95 nm compared to those reported for $[Fe^{III}(OO)(tpen)]^{+}$, $[Fe^{III}(OO)(metpen)]^{+}$, and $[Fe^{III}(OO)(bztpen)]^{+}$, respectively. The larger difference for the peroxido complexes may be related to the intramolecular H-bonding.

Competition between H_2O_2 disproportionation and ligand decomposition

A large excess (20–50 equiv with respect to iron) of H_2O_2 is required to generate maximum steady-state concentrations of $[Fe(OOH)(tpenaH)]^{2+}$ and $[Fe(OO)(tpenaH)]^{+}$, under which conditions evolution of gas is observed. Analysis of the dissolved and evolved volatiles by means of membrane inlet mass spectrometry (MIMS) and head-space Raman spectroscopy (HS-RS; $\lambda_{exc}=532$ nm) confirmed that the gas evolved was predominantly O_2. Addition of ^{18}O-labelled water in a 1:1:1 ratio of H_2O_2:$H_2{}^{16}O$:$H_2{}^{18}O$ mixture, confirmed that the O_2 evolved did not contain ^{18}O and hence that the two oxygen atoms in the evolved O_2 were derived from H_2O_2. Thus, $[Fe^{III}(tpena)]^{2+}$ catalyses H_2O_2 disproportionation rather than a more demanding oxidation of water.[28] To the best of our knowledge, H_2O_2 disproportionation catalysed by exclusively N-donor Rtpen-supported iron(III) peroxides (Scheme 2a; R = CH_3, $PyCH_2$) has not been reported.[10,11,17,29] Since it seemed plausible that this reaction had simply been overlooked (because bubbles were not visible) in previous studies of the generation of non-heme Fe^{III}-peroxides, we checked for this possible reaction in the present study by applying MIMS to monitor the reactions of $[Fe(Cl)(metpen)]^{+}$ and $[Fe(tpen)]^{2+}$ with 50 equiv of H_2O_2. We can verify that O_2 evolution, and hence catalase activity, does not occur as a side reaction when these exclusively N-donor ligands support the peroxide complexes.

In further contrast to the exclusively N-donor-supported iron peroxide complexes, the hydroperoxido species, $[Fe(OOH)(tpenaH)]^{2+}$, is not regenerated by the addition of a second portion (50 equiv) of H_2O_2 after the cessation of O_2 evolution, nor does catalytic H_2O_2 disproportionation resume. These observations indicate that either the catalyst is decomposed by H_2O_2 when the concentration of H_2O_2 is sufficiently low for competing C–H oxidation of the tpena ligand to become kinetically competent, or the increase in water concentration (introduced with and formed from H_2O_2) drives the formation of a kinetically inert oxido-bridged species $[(tpenaH)Fe(\mu\text{-}O)Fe(tpenaH)]^{4+}$.[24,30] To determine which of these pathways is pertinent, two equivalents of H_2O_2 were added to solutions of $[Fe(tpena)]^{2+}$ in acetonitrile. A colour change to purple was not observed. Head-space infrared spectroscopy (HS-IRS), however, showed that CO_2 was produced. The only carbon sources available for CO_2 production were the solvent acetonitrile and/or tpena. Monitoring both the O_2 and CO_2 releases by MIMS (Figure 5a) following the addition of 50 equiv of H_2O_2 revealed that O_2 was predominantly released in the early stages of the reaction. Quantitative analysis of the CO_2 release by HS-IRS showed that approximately seven CO_2 molecules per iron centre (Figure 5b) were produced. Increasing the amount of H_2O_2 added did not result in an increase in CO_2 formation, and it can therefore be concluded that the source of CO_2 was degradation of tpena rather than oxidation of acetonitrile. Specifically, the CO_2 must be derived from the aliphatic and carboxylate carbon atoms of tpenaH, as would be expected for aliphatic C–N oxidative cleavage/hydrolysis reactions.

The changes in iron speciation after the addition of 50 equiv of H_2O_2 were monitored by UV/Vis absorption, Raman, EPR, and Mössbauer spectroscopies. The band at 520 nm due to the purple $[Fe^{III}(OOH)(tpenaH)]^{2+}$ chromophore decayed completely, and then a new and more intense band appeared at 469 nm (Figure 6a). The absence of an isosbestic point suggests that the conversion between these iron-based chromophores involves relatively long-lived intermediates that do not absorb in the visible region. Time-resolved head-space FTIR and UV/Vis absorption data indicated that the growth of the band at 469 nm was concomitant with the release of CO_2 and the consequent growth of the absorbance at 2360 cm^{-1} in the HS-IR spectra. A fit of an EPR spectrum recorded from a reac-

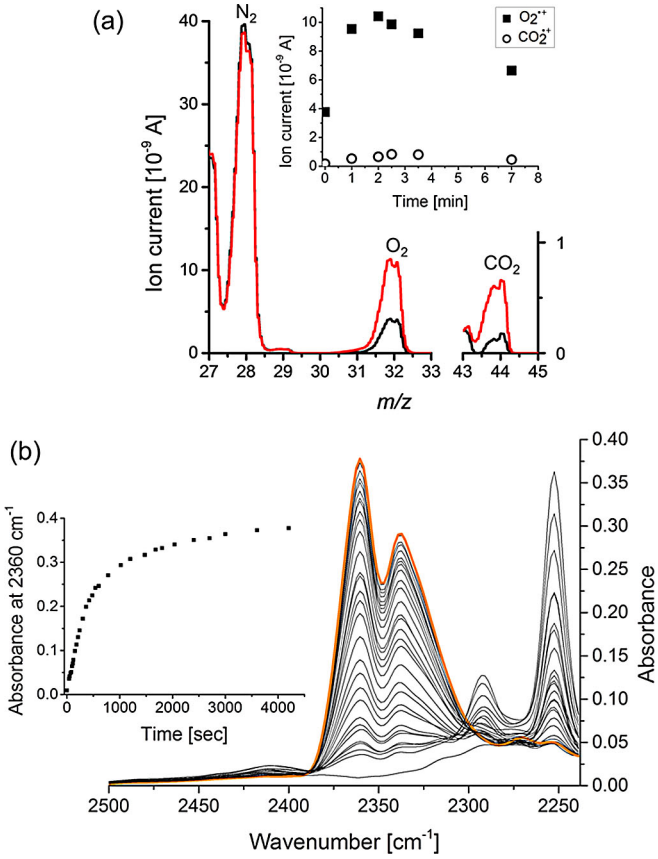

Figure 5. Detection of O_2 and CO_2 release. a) MIMS spectra of $[Fe(tpena)]^{2+}$ (0.5 mM in acetonitrile) (black) and 2 min after addition of 50 equiv of H_2O_2 (red). *m/z* 33–43 is omitted due to dominating intense MeCN signals (full spectrum: Supporting Information Figure S1). Inset: Time dependence of the ion current for the ions $O_2^{\cdot+}$ (*m/z* 32) and $CO_2^{\cdot+}$ (*m/z* 44). b) Time-resolved head-space FTIR spectroscopy showing evolution of CO_2 upon reaction of $[Fe(tpena)]^{2+}$ (2 mM) with 50 equiv of H_2O_2. Inset: Time dependence of absorbance at 2360 cm^{-1}. The acetonitrile bands at 2253 and 2292 cm^{-1} settle over time, concomitant with the decrease of effervescence due to both CO_2 and O_2.

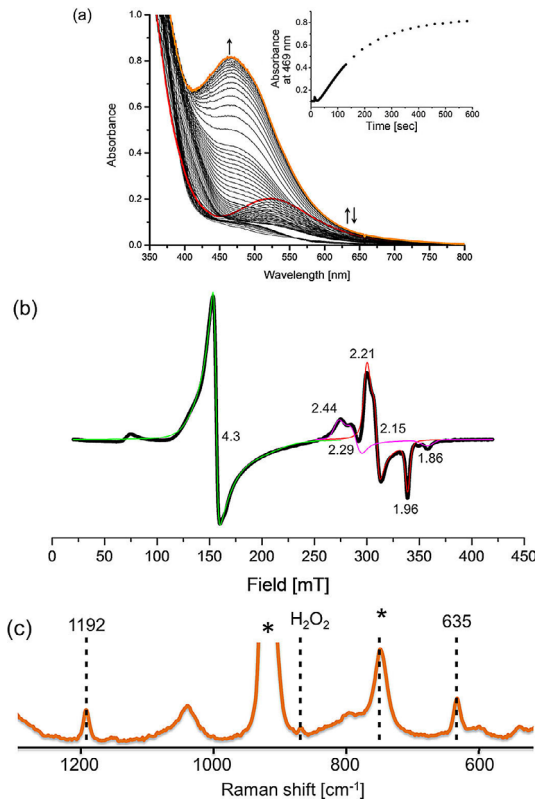

Figure 6. Time-resolved conversion of $[Fe^{III}(OOH)(tpenaH)]^{+}$ (red) to a low-spin Fe^{II} species (orange) with the addition of 50 equiv of H_2O_2. a) UV/Vis absorption spectroscopy. [Fe] = 0.5 mM. b) EPR spectrum recorded 2 min after the addition of H_2O_2 (black). Fitted data of $[Fe(OOH)(tpenaH)]^{2+}$ (red), a low-spin iron(III) species (pink, g = 2.44, 2.29, 1.86), and a high-spin iron(III) species (green, g^{eff} = 4.3). See Supporting Information Figure S3 for a summarized fit. c) Resonance Raman spectrum (λ_{exc} = 532 nm) recorded after the appearance of the absorption band at 469 nm. [Fe] = 1 mM, * = solvent bands.

tion mixture frozen at 110 K at 2 min after mixing of 50 equiv of aqueous H_2O_2 with $[Fe(tpena)]^{2+}$ showed three overlapping signals: a residual rhombic signal assigned to $[Fe(OOH)(tpenaH)]^{2+}$ (g = 2.21, 2.15, 1.96), a second broad rhombic signal assigned to an unknown low-spin iron(III) species at g = 2.44, 2.29, 1.86, and a signal at g^{eff} = 4.3 due to an unknown high-spin iron(III) species (Figure 6b). It is important to note, however, that all of these species appeared with significantly lower signal intensities compared to that for $[Fe(OOH)(tpenaH)]^{2+}$ recorded from a sample that was frozen seconds after mixing (Figure 3c). A series of spectra was recorded from the sample by allowing it to repeatedly warm to room temperature and then re-freezing it for EPR spectral acquisition in order to provide snapshots of the formation and disappearance of the aforementioned signals. A final spectrum was recorded after the solution had been left to stand for 2 h at room temperature. This showed that only a trace amount of the high-spin Fe^{III} signal remained, with the loss of all other signals. The Mössbauer spectrum recorded on the mixture containing $[Fe(OOH)(tpenaH)]^{2+}$ (Figure 3d) shows, along with signals for $[Fe(OOH)(tpenaH)]^{2+}$ (red) and $[Fe_2O(tpenaH)_2]^{4+}$ (green) a large area ascribed to one or more unidentified species. For simplicity, this was fitted to a broad asymmetric doublet with $\delta \approx$ 0.20 mm s^{-1} and $\Delta E_Q \approx$ 1.90 mm^{-1} (72%, orange fit). Such asymmetric doublets are commonly seen in spectra of high-spin iron(III) species with paramagnetic relaxation times on the order of a nanosecond. The low intensity of the signal in corresponding EPR spectra suggests that the electron spin relaxation in this dominant non-integer spin component is too rapid for the EPR timescale. Other potential decomposition products, integer spin Fe^{II} and Fe^{IV} monomers and the strongly anti-ferromagnetically coupled starting material, $[Fe_2O(tpenaH)_2]^{4+}$, are expected to be EPR silent. Bands at ν = 634, 1192, and 2094 cm^{-1} appeared in the Raman spectrum (λ_{exc} = 532 nm) of equivalently treated solutions (Figure 6c). The band at ν = 2094 cm^{-1} is consistent with the presence of Fe^{II}-coordinated acetonitrile.[31] A ^{1}H NMR spectrum of the reaction mixture in CD_3CN recorded after 16 h (and hence coinciding with the presence of the EPR-silent species with an absorption at 469 nm showed the characteristic signal of NH_3 (three resonances of equal intensity centred at δ = 6.61 ppm, $J_{14N\text{-}1H}$ = 52 Hz; Supporting Information, Figure S2). This demonstrated that the production of NH_3 occurred concomitantly with the production of tpenaH-derived CO_2. The signals remaining in the aromatic region (7–9 ppm) suggested that the pyridine groups remained intact. Positive- and negative-ion ESI-MS did not provide evidence for the formation of a complex with pyridine ligands that might be associated with the species at 469 nm. Indirectly, however, the ESI-MS data provide further evidence that all of the aliphatic C atoms of the ligands were converted into CO_2 through the absence, for example, of picolinato complexes that have previously been observed to form through the reaction of aminopyridyl-metal complexes with peroxides.[32] Overall, the data lead to the conclusion that reaction of $[Fe(tpena)]^{2+}$ with a large excess of H_2O_2 results primarily in H_2O_2 disproportionation, but is accompanied by concurrent oxidative decay of the tpena ligand, which occurs *primarily when the concentration of H_2O_2 is low.* A mixture of heteroleptic iron(II) complexes of pyridine, ammonia, and/or acetonitrile ligands is ultimately formed through the oxidative decomposition of $[Fe^{III}(tpena)]^{2+}$.

Catalytic alcohol oxidation overrides catalase activity and ligand decomposition

In stark contrast to the reactions of $[Fe^{II}(Cl)(Rtpena)]^{+}$ with excess H_2O_2 in methanol,[10,11,17] the addition of 50 equiv of H_2O_2 to solutions of $[Fe^{III}(tpena)]^{2+}$ in methanol does not give rise to detectable amounts of purple $[Fe^{III}(OOH)(tpenaH)]^{2+}$. This is because methanol is oxidized. Analysis using the Hantzsche reaction[33] and UV/Vis absorption spectroscopy showed that formaldehyde was produced in approximately 35% yield based on the initial H_2O_2 concentration. Thus, the activation of H_2O_2 by $[Fe^{III}(tpena)]^{2+}$ can be directed to perform substrate oxidation. This observation inspired us to examine a more readily oxidizable substrate, benzyl alcohol, in acetonitrile (bond dissociation energies for H–CH_2OH and H–CH(OH)Ph are 96 and 79 kcal mol^{-1}, respectively[34]). The addition of 50 equiv of H_2O_2 to $[Fe(tpena)]^{2+}$ in the presence of 500 equiv of benzyl alcohol did not result in either O_2 or CO_2 evolution, and hence

neither H_2O_2 disproportionation nor tpena decomposition occurred. In contrast to the reactions performed in methanol, under these conditions, $[Fe^{III}(OOH)(tpenaH)]^{2+}$ was observed spectroscopically due to the lower concentration of the alcohol substrate. The addition of a second portion of H_2O_2 (50 equiv) resulted in reappearance of the absorption band of $[Fe^{III}(OOH)(tpenaH)]^{2+}$ with the same intensity as after the first addition (Figure 7). Continued batchwise addition of H_2O_2

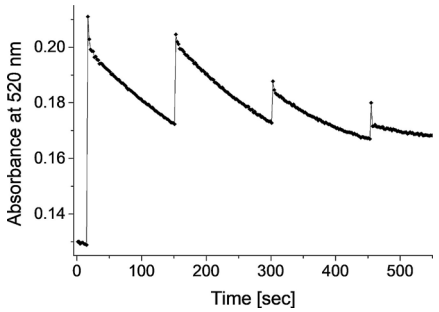

Figure 7. Time dependence of the absorbance at 520 nm in the presence of 500 equiv of $PhCH_2OH$ ([Fe] = 0.5 mM). The batchwise addition of 50 equiv of H_2O_2 causes jumps in the absorbance due to formation of the Fe^{III}-OOH intermediate.

eventually led to decomposition of the ligand, that is, the band at 469 nm intensified and the purple colour, due to $[Fe^{III}(OOH)(tpenaH)]^{2+}$, was lost. Thus, tpenaH oxidation competes with alcohol oxidation and the presence of a large excess of alcohol, or its use as the solvent delays the onset of ligand oxidation. ^{1}H NMR spectroscopic analysis showed, after five additions of 50 equiv of H_2O_2 over 10 min, 50% conversion of benzyl alcohol to benzaldehyde and hence near-stoichiometric conversion with respect to the oxidant. A control reaction in the absence of $[Fe(tpena)]^{2+}$ showed that, under otherwise identical conditions, benzyl alcohol was oxidized by H_2O_2 with only 32% conversion after 20 h.[35]

Mechanistic considerations

The reaction of $[(tpenaH)Fe\text{-}O\text{-}Fe(tpenaH)]^{4+}$ with Ce^{IV} in water produces the iron(IV) oxo complex, $[Fe^{IV}(O)(tpenaH)]^{2+}$,[24] and recently we have generated this same species electrochemically, also in water.[23] In both of these studies, we demonstrated $[Fe^{IV}(O)(tpenaH)]^{2+}$ to be a promiscuous oxidant in the absence of hydroxyl radicals. It attacks a broad range of C–H bonds by hydrogen-atom transfer. Thus, $[Fe^{IV}(O)(tpenaH)]^{2+}$ displays radical character. Calculations by Faponle et al. show that $[Fe^{IV}{=}O(metpen)]^{2+}$ can be generated by homolytic cleavage of $[Fe(OOH)(metpen)]^{2+}$, and it is the Fe^{IV} oxo species that reacts with substrates.[36] This reaction has been demonstrated in the gas phase.[11] However, the phase of the reaction medium (and second coordination sphere) is likely to tune the O–O bond-cleavage reaction. With these facts in mind, we propose that the H_2O_2 activation and reactivity described in the present study can be rationalized in terms of homolytic O–O bond cleavage of the hydroperoxide ligand in $[Fe^{III}(OOH)(tpenaH)]^{2+}$. This reactivity is in contrast to the behaviour of Fe^{III}-OOH based on neutral N5 donor systems. In fact, peroxide dissociation[17,29] is a highly competitive pathway for the decomposition of $(N5)Fe^{III}$-OOH species. It can thus be concluded that for the iron-tpena system, homolytic O–O bond cleavage occurs in $[Fe^{III}(OOH)(tpenaH)]^{2+}$, resulting in the formation of $[Fe^{IV}(O)(tpenaH)]^{2+}$ and a hydroxyl radical. Both are aggressive hydrogen-atom abstractors and will react with methanol, benzyl alcohol, and hydrogen peroxide to form the methanoyl, benzoyl, and hydroperoxide ($^{\bullet}CH_2OH$, $C_6H_5{}^{\bullet}CHOH$, $^{\bullet}OOH$) radicals, respectively. In turn, these radicals will propagate chain reactions and radical terminations to give the detected products, CH_2O, C_6H_5CHO, and O_2. Interconnected catalytic cycles for H_2O_2 disproportionation and alcohol oxidation are proposed in Scheme 6.

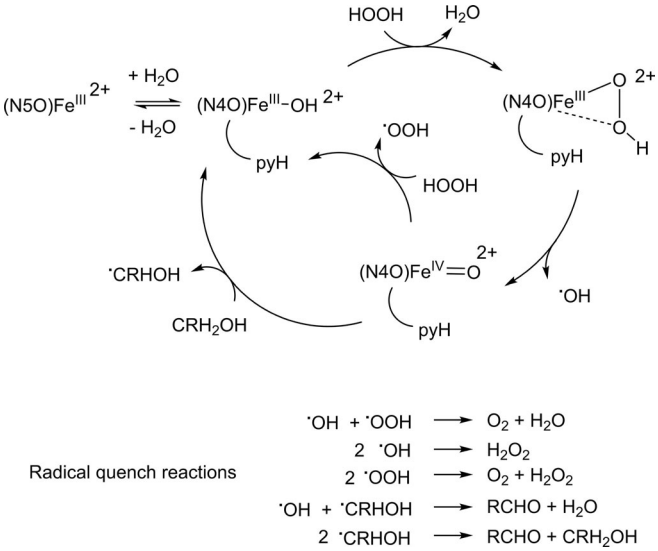

Scheme 6. Connected catalytic cycles for H_2O_2 disproportionation and O_2 evolution, as well as methanol (R = H) and benzyl alcohol (R = C_6H_5) oxidation by H_2O_2.

Perspective on the tunability by varying the supporting ligand in H_2O_2 activation by non-heme iron complexes

Compared to analogous iron(III)-hydroperoxide complexes based on supporting N5 and N6 ligands containing exclusively pyridine and tertiary amine donors (Scheme 2a) and analogous *N*,*N*-bis(2-pyridylmethyl)-*N*-bis(2-pyridyl)methylamine[37] (N4py) systems, the influence of a biomimetic carboxylato donor is demonstrated by the significant difference in Fe^{III}/Fe^{II} redox potentials of the parent $[Fe(tpen)]^{3+}$ and $[Fe(tpena)]^{2+}$ complexes. The latter is shifted to lower values by an average of 360 mV for the diastereoisomers in acetonitrile. A practical consequence of the lower redox potential is that tpena-Fe^{III} complexes are isolated, and these are redox-stable in the +3 oxidation state in all solvents examined.[20,21] This result stands in contrast to observations for the complexes of tpen and related N5 neutral pentadentate ligands (Scheme 2a), for which the iron(II) complexes are those most readily isolated, especially in solvents such as acetonitrile. These are thermodynamic sinks,

retarding their reactivity with H_2O_2. This tendency towards greater stability in higher iron oxidation states will have a significant impact on the chemistry of the iron-tpena complexes and hence on the construction of proposed catalytic cycles. The pro-catalyst and resting state is iron(III) and not iron(II). As such, the process of peroxide adduct formation does not require a prior oxidation step from iron(II) to iron(III). The Fe^{IV}/Fe^{III} couple can be reasonably expected to follow this trend towards lower potentials,[38] and this will favour promotion of the homolytic cleavage of the $Fe^{III}O$–OH bond in the hydroperoxide adduct to readily attain an iron(IV) oxo species. This is manifested in significantly shorter lifetimes for $[Fe(OOH)(tpenaH)]^{2+}$ and $[Fe(OO)(tpenaH)]^{+}$ compared to the corresponding systems based on N5/N6 Rtpen ligands. A further contrast to the N5/N6 donor-supported systems for the reaction of H_2O_2 with the resting state iron(III) in $[Fe(tpena)]^{2+}$ is that no deprotonation of the H_2O_2 is needed. It is an addition reaction accompanied by charge separation due to concomitant pyridine decoordination and pyridinium formation. The ligand is converted from monoanionic hexadentate (tpena) to zwitteranionic pentadentate (tpenaH). With one carboxylato donor and a second base in the coordination sphere, $[Fe(OOH)(tpenaH)]^{2+}$ and its conjugate base $[Fe(OO)(tpenaH)]^{+}$ are particularly germane biomimics for non-heme iron(III) peroxides. The peroxide activation chemistry that we have observed is pertinent to elucidating mechanisms for O_2-activating enzymes in which Gly/Asp groups are coordinated to the O_2-binding site on iron.[9] In particular, we note that the non-heme 1 Asp/3 His-coordinated iron superoxide dismutase[39] evolves O_2 in a similar manner to the Fe-tpena system studied here (although the disproportionated substrate is $O_2^{\bullet-}$ and not H_2O_2). The basic amino acid residues found in the second coordination sphere of non-heme active sites are proposed to facilitate proton-coupled redox reactions, and a similar role for the dangling pyridine/pyridinium groups of the tpena system is feasible.

The contrast in peroxide activation reactivity between $[Fe(tpena)]^{2+}$ and the parent pentadentate N4O Rbpena-based Fe^{III} systems (Scheme 2b) described in the Introduction is also worth noting: ligand oxygenations result from reactions of the iron(III) starting complexes with H_2O_2, without the detection of intermediate peroxide adducts (Scheme 2b). The two types of O atom insertions observed are consistent with heterolytic O–O cleavage of a putative (Rbpena)Fe^{III}O–O(H) intermediate to form a putative Fe^{V} oxo species. This reactive species can then transfer [O] to the aromatic C–H or N in bzbpena and mebpena, respectively. The iron(III) complexes of the modified "RbpenaO" ligands may be unable to activate H_2O_2, and are therewith stable towards oxidative decomposition, in contrast to the iron complex of tpena.[18] Interestingly, the manganese complexes of Rbpena and tpena can withstand thousands of equivalents of organic peroxides without decomposition or ligand modification.[26,28]

Conclusions

Methanol oxidation to formaldehyde and stoichiometric yields of benzaldehyde from the $[Fe(tpena)]^{2+}$-catalysed oxidation of benzyl alcohol by H_2O_2 have been realized in the present study. In the absence of a large excess of a second substrate, H_2O_2 disproportionation is catalysed by $[Fe(tpena)]^{2+}$ through a related mechanism. However, in the absence of other oxidizable substrates (methanol, benzyl alcohol, and H_2O_2), oxidative decay of $[Fe(tpena)]^{2+}$ occurs through the spectroscopically detectable intermediate $[Fe(OOH)(tpenaH)]^{2+}$. Release of all of the aliphatic carbon atoms and amine groups as CO_2 and NH_3, respectively, has been demonstrated. The reactivity patterns observed (catalysis of the oxidation of alcohols, catalase activity, and tpena degradation, Scheme 3) reflect the higher C–H bond strength in MeCN compared to MeOH, the aliphatic C–H bonds in tpena, and the O–H bond in H_2O_2, respectively. Overall, the H_2O_2 activation chemistry described here stands in contrast to that reported previously for the pentadentate N5 supporting ligands $[Fe^{III}(OOH)(Rtpen)]^{2+}$ and $[Fe^{III}(OOH)(N4py)]^{2+}$ and a carboxylate-containing N4O pentadentate supporting ligand $[Fe^{III}(OOH)(Rbpena)]^{2+}$. We have shown: 1) facile homolytic Fe^{III}O–OH cleavage in solution to produce two aggressive H-atom abstractors, Fe^{IV}=O and $HO^{\bullet}$, 2) catalytic H_2O_2 disproportionation, 3) catalytic alcohol oxidation with stoichiometric yields, and 4) total destruction of the aliphatic part of tpena in the presence of low concentrations of H_2O_2. By tuning the penta- and hexadentate ethylenediamine-backboned ligands (Scheme 2), a tendency towards the limiting reaction types depicted in Equations (2), (3), and (4) for Fe^{III}-peroxide adducts has been exposed. It seems that H_2O_2 activation is more effective for the carboxylato ligands and the difference in reactivity seen for the N4O (Rbpena) and N5O (tpena) ligand systems must be due to the availability of a second base in the coordination sphere for the latter. The proximity of this group suggests that it may participate at many stages, from its decoordination to allow adduct formation by charge-separated H_2O_2 addition to H-bonding in the peroxide intermediates. In turn, this electronic modulation may effect a homolytic O–O cleavage rather than the heterolytic cleavage and intramolecular oxygenation that occurs with the otherwise stereochemically and electronically similar N4O Rbpena as a supporting ligand.

Dissociation:

$$[Fe^{III}(OOH)(Rtpen)]^{2+} + HX \rightleftharpoons [Fe^{III}(X)(Rtpen)]^{2+} + HOOH \quad (2)$$

O–O heterolysis:

$$[Fe^{III}(OOH)(Rbpena)]^{2+} \rightarrow [Fe^{III}(RbpenaO)]^{2+} + OH^{-} \quad (3)$$

O–O homolysis:

$$[Fe^{III}(OOH)(tpenaH)]^{2+} \rightarrow [Fe^{IV}(O)(tpenaH)]^{2+} + OH^{\bullet} \quad (4)$$

Our work not only presents a germane mimic for non-heme iron chemistry, especially in terms of the carboxylato group and the second coordination sphere base, but also adds to our knowledge of the ligand design features important for activating H_2O_2, demonstrates controllable bifurcation in catalysed external substrate oxidation reactions, and indicates that destruc-

tive oxidation of the supporting ligand can be avoided through appropriate experimental design [Eqs. (2–4)].

Experimental Section

Materials and preparations

N,N,N'-Tris-(2-pyridylmethyl)ethylenediamine-*N'*-acetic acid (tpenaH),[40] [(tpenaH)Fe-O-Fe(tpenaH)]$(ClO_4)_4(H_2O)_2$,[20] [Fe(Cl)-tpen](PF_6),[17] [Fe(Cl)metpen)](PF_6),[17] and [Fe(tpen)]$(ClO_4)_2$[41] were prepared as described previously. [^{18}O]H_2O was supplied by Rotem Industries Ltd., and all other chemicals were purchased from Sigma-Aldrich.

CAUTION!!! Perchlorate salts of metal complexes are potentially explosive and should be handled with caution in small quantities.

[Fe(OOH)(tpenaH)]$^{2+}$ and [Fe(OO)(tpenaH)]$^{+}$: [(tpenaH)Fe-O-Fe-(tpenaH)]$(ClO_4)_4(H_2O)_2$ was dissolved in acetonitrile and the solution was allowed to stand for 10 min until [(tpenaH)Fe-O-Fe(tpenaH)]$^{4+}$ had dehydrated to [Fe(tpena)]$^{2+}$. This solution was then treated with 50 equiv of H_2O_2 (50% in water, w/w) to give [Fe(OOH)-(tpenaH)]$^{2+}$, and [Fe(OO)(tpenaH)]$^{+}$ was formed by the subsequent addition of 30 equiv of Et_3N.

[Fe(Cl)(tpenaH)]$(ClO_4)_2$·(EtOH)·2(H_2O): $Fe(ClO_4)_2$·6H_2O (773 mg, 1.7 mmol) was added to tpenaH (655 mg, 1.7 mmol) in acetonitrile (5 mL), water (5 mL), and ethanol (5 mL), and the mixture was adjusted to pH 3 with HCl(aq.). Upon slow evaporation of the volatiles, yellow crystals of [Fe(Cl)(tpenaH)]$(ClO_4)_2$·EtOH·2H_2O (702 mg, 54%) were deposited after two weeks. ESI-MS (MeCN): *m/z*: 479.1 ([Fe(Cl)(tpena−2H)]$^{+}$, 78%), 481.1 ([Fe(Cl)(tpena)]$^{+}$, 81%), 482.1 ([Fe(Cl)(tpenaH)]$^{+}$, 100%); ESI-MS (H_2O): *m/z*: 446.1 ([Fe(tpena)]$^{+}$, 34%), 454.1 ([(tpena)Fe-O-Fe(tpena)]$^{2+}$, 100%), 463.1 ([Fe(OH)-(tpena)]$^{+}$, 85%); IR (KBr): $\nu = 1610$ (C=O, s), 1098 cm^{-1} (ClO_4^{-}, vs); elemental analysis calcd (%) for $C_{22}H_{29}N_5O_{12}Cl_3Fe$ ([Fe(Cl)(tpenaH)]-$(ClO_4)_2$·2H_2O: C 36.82, H 4.07, N 9.76; found: C 36.21, H 3.65, N 9.27.

Instrumentation and methods

UV/Vis spectra were recorded from solutions in 1 cm quartz cuvettes on either an Agilent 8453 spectrophotometer with a UNISO-KU CoolSpeK UV USP-203 temperature controller or an Analytik Jena Specord S600 with a Quantum Northwest TC 125 temperature controller. Raman spectra were recorded from samples in 1 cm quartz cuvettes at either 532 nm (300 mW at source, Cobolt Lasers) as described previously[30] or 691 nm (75 mW at sample, Ondax Lasers). The solutions were cooled with a Quantum Northwest TC 125 temperature controller and the spectra were obtained at −30 °C. Data were recorded and processed using Solis (Andor Technology) with spectral calibration with respect to the Raman spectrum of MeCN/toluene (50:50, w/w). Baseline correction was performed for all spectra, and normalized to the solvent band at 750 cm^{-1}. EPR spectra (X-band) were recorded on a Bruker EMX Plus CW spectrometer (mod. amp.: 10 G, attenuation: 10 dB) on frozen solutions at 110 K. In order to follow the decay of the iron species, the samples for measurements (200 μL) were transferred to EPR tubes and frozen in liquid nitrogen at different times. The software packages eview4wr and esimX were used for simulation.[42] ^{1}H NMR (400.12 MHz) spectra were recorded on a Bruker Avance III 400 spectrometer at ambient temperature. Chemical shifts are denoted relative to the residual solvent peak (CD_3CN, 1.94 ppm). Mössbauer spectra were obtained with conventional constant acceleration spectrometers with sources of ^{57}Co in rhodium foil. The spectra were collected at 14 K. Isomer shifts are given relative to that of α-Fe at 295 K. Infrared spectra (IR) were obtained on a Hitachi 270-30 IR spectrometer from samples in KBr pellets. Head-space FTIR spectra were recorded from samples in sealed 1 cm quartz cuvettes on a JASCO FT-NIR/MIR-4600 spectrometer with a resolution of 8 cm^{-1}. The concentration of CO_2 released was quantified on the basis of standard solutions of Na_2CO_3 in water with addition of 3 equiv acid (HCl) to force the release of CO_2. Aliquots (1 mL) of the solution were placed in a sealed cuvette, and the head-space was monitored before and after the addition of acid. A standard curve based on the absorbance at 2360 cm^{-1} was fitted to [CO_2] < 5 mM: Abs (2360 cm^{-1}) = 0.0300 mM^{-1}· [CO_2] + 0.0084 and [CO_2] > 5 mM: Abs (2360 cm^{-1}) = 0.0281 mM^{-1}· [CO_2] + 0.0213. MIMS spectra were recorded using a Prisma quadrupole mass spectrometer (Pfeiffer Vacuum, Asslar, Germany). A flat sheet membrane (250 μm) of polydimethyl siloxane (Sil-Tec sheeting, Technical Products, Decatur, GA, USA) separated the vacuum chamber (1×10^{-6} mbar) from the solution in the sample chamber (total volume 2.5 mL), which was stirred mechanically. The data were recorded and processed using Quadstar 422 (Pfeiffer Vacuum, Asslar, Germany). The reaction chamber was filled with a solution of [Fe-(tpena)]$^{2+}$, and H_2O_2 was injected directly into the solution in the sample chamber as the resulting gas evolution was simultaneously measured. Electrospray ionization (ESI) mass spectra were recorded in high-resolution positive-ion mode on a Bruker microTOF-QII mass spectrometer. Single-crystal X-ray diffraction data were collected on a Rigaku R-AXIS IIC image-plate system ($Mo_{K\alpha}$ radiation) at 100 K. Cyclic voltammetry was performed on an Eco Chemie Autolab PGSTAT10 potentiostat/galvanostat using a standard three-electrode set-up with a Pt disc as the working electrode, a Pt wire as the counter electrode, and Ag/Ag^{+} as the reference electrode (0.01 M $AgNO_3$ in 0.1 M $TBAClO_4$ in MeCN; TBA: *tert*-butylammonium). The electrolyte was also 0.1 M $TBAClO_4$ in MeCN. The working electrode was cleaned by polishing with 0.05 μm alumina followed by sonication, and the solutions were purged with nitrogen prior to measurements. The oxidation potential of Fc/Fc^{+} against Ag/Ag^{+} was measured as 0.08 V, and all oxidation potentials were converted accordingly.

CCDC 1559278 ([Fe(Cl)(tpenaH)]$(ClO_4)_2$·(EtOH)·2(H_2O)) contains the supplementary crystallographic data for this paper. These data are provided free of charge by The Cambridge Crystallographic Data Centre.

Acknowledgements

This work was supported by the Danish Council for Independent Research | Natural Sciences (grant 4181-00329 to C.McK.). C.W. thanks COST action CM1305 (ECOSTBio) for the travel grant STSM #30679. Dr. Anne Nielsen, Dr. Anders Lennartson, and Dr. Mads Vad are acknowledged for some preliminary experimental work. Lars Brændegaard Hansen is thanked for designing the reaction cell for the MIMS setup.

Conflict of interest

The authors declare no conflict of interest.

Keywords: H_2O_2 activation · high-valent iron · hydroxyl radical · iron(IV) · N,O ligands · peroxides

[1] B. Meunier, S. P. de Visser, S. Shaik, *Chem. Rev.* **2004**, *104*, 3947–3980.

[2] J. H. Dawson, *Science* **1988**, *240*, 433 – 439.
[3] M. Costas, M. P. Mehn, M. P. Jensen, L. Que, Jr., *Chem. Rev.* **2004**, *104*, 939 – 986.
[4] S. Kal, L. Que, Jr., *J. Biol. Inorg. Chem.* **2017**, *22*, 339 – 365.
[5] W. Nam, *Acc. Chem. Res.* **2015**, *48*, 2415 – 2423.
[6] K. P. Bryliakov, E. P. Talsi, *Coord. Chem. Rev.* **2014**, *276*, 73 – 96.
[7] L. Que, Jr., W. B. Tolman, *Nature* **2008**, *455*, 333 – 340.
[8] W. Nam, *Acc. Chem. Res.* **2007**, *40*, 522 – 531.
[9] E. G. Kovaleva, J. D. Lipscomb, *Nat. Chem. Biol.* **2008**, *4*, 186 – 193.
[10] I. Bernal, I. M. Jensen, K. B. Jensen, C. J. Mckenzie, H. Toftlund, J.-P. Tuchagues, *J. Chem. Soc. Dalton Trans.* **1995**, 3667 – 3675.
[11] K. B. Jensen, C. J. McKenzie, L. P. Nielsen, J. Z. Pedersen, H. M. Svendsen, *Chem. Commun.* **1999**, 1313 – 1314.
[12] A. J. Simaan, F. Banse, P. Mialane, A. Boussac, S. Un, T. Kargar-Grisel, G. Bouchoux, J.-J. Girerd, *Eur. J. Inorg. Chem.* **1999**, 993 – 996.
[13] P. Mialane, A. Nivorojkine, G. Pratviel, L. Azéma, M. Slany, F. Godde, A. Simaan, F. Banse, T. Kargar-Grisel, G. Bouchoux, J. Sainton, O. Horner, J. Guilhem, L. Tchertanova, B. Meunier, J.-J. Girerd, *Inorg. Chem.* **1999**, *38*, 1085 – 1092.
[14] A. J. Simaan, S. Döpner, F. Banse, S. Bourcier, G. Bouchoux, A. Boussac, P. Hildebrandt, J.-J. Girerd, *Eur. J. Inorg. Chem.* **2000**, 1627 – 1633.
[15] A. J. Simaan, F. Banse, J.-J. Girerd, K. Wieghardt, E. Bill, *Inorg. Chem.* **2001**, *40*, 6538 – 6540.
[16] O. Horner, C. Jeandey, J.-L. Oddou, P. Bonville, C. J. McKenzie, J.-M. Latour, *Eur. J. Inorg. Chem.* **2002**, 3278 – 3283.
[17] A. Hazell, C. J. McKenzie, L. P. Nielsen, S. Schindler, M. Weitzer, *J. Chem. Soc. Dalton Trans.* **2002**, 310 – 317.
[18] A. Nielsen, F. B. Larsen, A. D. Bond, C. J. McKenzie, *Angew. Chem. Int. Ed.* **2006**, *45*, 1602 – 1606; *Angew. Chem.* **2006**, *118*, 1632 – 1636.
[19] a) J. Kaizer, E. J. Klinker, N. Y. Oh, J.-U. Rohde, W. J. Song, A. Stubna, J. Kim, E. Münck, W. Nam, L. Que, Jr., *J. Am. Chem. Soc.* **2004**, *126*, 472 – 473; b) V. Balland, M.-F. Charlot, F. Banse, J.-J. Girerd, T. A. Mattioli, E. Bill, J.-F. Bartoli, P. Battioni, D. Mansuy, *Eur. J. Inorg. Chem.* **2004**, 301 – 308; c) M. Martinho, F. Banse, J.-F. Bartoli, T. A. Mattioli, P. Battioni, O. Horner, S. Bourcier, J.-J. Girerd, *Inorg. Chem.* **2005**, *44*, 9592 – 9596.
[20] A. Lennartson, C. J. McKenzie, *Angew. Chem. Int. Ed.* **2012**, *51*, 6767 – 6770; *Angew. Chem.* **2012**, *124*, 6871 – 6874.
[21] D. P. de Sousa, C. Wegeberg, M. S. Vad, S. Mørup, C. Frandsen, W. A. Donald, C. J. McKenzie, *Chem. Eur. J.* **2016**, *22*, 3810 – 3820.
[22] D. Angelone, D. Abdolahzadeh, J. W. de Boer, W. R. Browne, *Eur. J. Inorg. Chem.* **2015**, 3532 – 3542.
[23] D. P. de Sousa, C. J. Miller, Y. Chang, T. D. Waite, C. J. McKenzie, *Inorg. Chem.* **2017**, DOI: https://doi.org/10.1021/acs.inorgchem.7b02208.
[24] M. S. Vad, A. Lennartson, A. Nielsen, J. Harmer, J. E. McGrady, C. Frandsen, S. Mørup, C. J. McKenzie, *Chem. Commun.* **2012**, *48*, 10880 – 10882.
[25] D. P. de Sousa, J. O. Bigelow, J. Sundberg, L. Que, Jr., C. J. McKenzie, *Chem. Commun.* **2015**, *51*, 2802 – 2805.
[26] C. Deville, M. Finsel, D. P. de Sousa, B. Szafranowska, J. Behnken, S. Svane, A. D. Bond, R. K. Seidler-Egdal, C. J. McKenzie, *Eur. J. Inorg. Chem.* **2015**, 3543 – 3549.
[27] U. G. Nielsen, A. Hazell, J. Skibsted, H. J. Jakobsen, C. J. McKenzie, *CrystEngComm* **2010**, *12*, 2826 – 2834.
[28] a) A. K. Poulsen, A. Rompel, C. J. McKenzie, *Angew. Chem. Int. Ed.* **2005**, *44*, 6916 – 6920; *Angew. Chem.* **2005**, *117*, 7076 – 7080; b) R. K. Seidler-Egdal, A. Nielsen, A. D. Bond, M. J. Bjerrum, C. J. McKenzie, *Dalton Trans.* **2011**, *40*, 3849 – 3858.
[29] T. Nebe, A. Beitat, C. Würtele, C. Dücker-Benfer, R. van Eldik, C. J. McKenzie, S. Schindler, *Dalton Trans.* **2010**, *39*, 7768 – 7773.
[30] S. K. Padamati, A. Draksharapu, D. Unjaroen, W. R. Browne, *Inorg. Chem.* **2016**, *55*, 4211 – 4222.
[31] A. Boffi, E. Chiancone, *Biochemistry* **1997**, *36*, 4505 – 4509.
[32] a) C. Deville, V. McKee, C. J. McKenzie, *Dalton Trans.* **2017**, *46*, 709 – 719; b) D. Pijper, P. Saisaha, J. W. de Boer, R. Hoen, C. Smit, A. Meetsma, R. Hage, R. P. van Summeren, R. L. Alsters, B. L. Feringa, W. R. Browne, *Dalton Trans.* **2010**, *39*, 10375 – 10381.
[33] T. Nash, *Biochem. J.* **1953**, *55*, 416 – 421.
[34] Y.-R. Luo, in *Comprehensive Handbook of Chemical Bond Energies*, CRC, Boca Raton, **2007**, pp. 19 – 134.
[35] A control using $[Fe(tpen)]^{2+}$ actually showed a decrease in the rate of benzyl alcohol oxidation compared to the non-catalysed reaction. This implies that the coordination of the hydroperoxide to form $[Fe(OOH)tpen)]^{2+}$ in fact results in a deactivation of H_2O_2, at least with respect to this particular reaction.
[36] A. Faponle, M. G. Quesne, C. V. Sastri, F. Banse, S. P. de Visser, *Chem. Eur. J.* **2015**, *21*, 1221 – 1236.
[37] a) M. Lubben, A. Meetsma, E. C. Wilkinson, B. Feringa, L. Que, Jr., *Angew. Chem. Int. Ed. Engl.* **1995**, *34*, 1512 – 1514; *Angew. Chem.* **1995**, *107*, 1610 – 1612; b) G. Roelfes, M. Lubben, K. Chen, R. Y. N. Ho, A. Meetsma, S. Genseberger, R. M. Hermant, R. Hage, S. K. Mandel, V. G. Young, Jr., Y. Zang, H. Kooijman, A. L. Spek, L. Que, Jr., B. L. Feringa, *Inorg. Chem.* **1999**, *38*, 1929 – 1936.
[38] Although not directly comparable, we have observed the oxidation of $[(tpenaH)Fe^{III}(\mu\text{-}O)Fe^{III}(tpenaH)]^{4+}$ in water to give $[Fe^{IV}(O)\text{-}(tpenaH)]^{2+}$ to occur at around 500–670 mV versus the NHE in the pH range 7–2, respectively. See reference [23].
[39] M. S. Lah, M. M. Dixon, K. A. Pattridge, W. C. Stallings, J. A. Fee, M. L. Ludwig, *Biochemistry* **1995**, *34*, 1646 – 1660.
[40] J. Glerup, P. A. Goodson, A. Hazell, R. Hazell, D. J. Hodgson, C. J. McKenzie, K. Michelsen, U. Rychlewska, H. Toftlund, *Inorg. Chem.* **1994**, *33*, 4105 – 4111.
[41] H.-R. Chang, J. K. McCusker, H. Toftlund, S. R. Wilson, A. X. Trautwein, H. Winkler, D. N. Hendrikson, *J. Am. Chem. Soc.* **1990**, *112*, 6814 – 6827.
[42] E. Bill 2016, Max-Planck-Institute for Chemical Energy Conversion, Mülheim; available from the author by mail to: eckhard.bill@cec.mpg.de.

Manuscript received: September 29, 2017
Accepted manuscript online: October 30, 2017
Version of record online: ■■ ▮▮, 0000

FULL PAPER

Peroxide activation at Fe: A transient Fe^{III}-hydroperoxide intermediate has been spectroscopically identified during $[Fe^{III}(tpena)]^{2+}$-catalysed H_2O_2 disproportionation in acetonitrile (see graphic). If benzyl alcohol is present, or methanol is used as solvent, H_2O_2 disproportionation is inhibited in favour of high-yielding alcohol oxidation to the corresponding aldehyde. In the absence of excess substrate (alcohol or H_2O_2), tpena is oxidatively degraded.

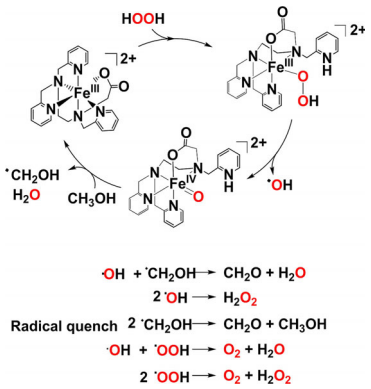

Coordination Chemistry

*C. Wegeberg, F. R. Lauritsen, C. Frandsen, S. Mørup, W. R. Browne, C. J. McKenzie**

■■ – ■■

Directing a Non-Heme Iron(III)-Hydroperoxide Species on a Trifurcated Reactivity Pathway